International Journal on Smart Material and Mechatronics
IJSMM Vol. 2 No. 2 2015

p-ISSN: 2356-5314
e-ISSN: 2460-075X

Obstacle Avoidance for Autonomous Locomotion of a Quadrotor Using an HPF

Kimiko Motonaka, Keigo Watanabe, and Shoichi Maeyama
Graduate School of Natural Science and Technology
Okayama University
Okayama, Japan
k.motonaka@usmm.sys.okayama-u.ac.jp

Received: 15 September 2015 / Revised: 10 October 2015 / Accepted: 26 October 2015 / Published online: 10 January 2016

***Abstract*— There is a concept called "kinodynamic motion planning" which can consider kinematic constraints and dynamic constraints simultaneously. In this paper, we test the proposed kinodynamic motion planning, which was confirmed in only simulations, by an actual experiment. The experiment assumes that the quadrotor moves in the static environment, and it is confirmed that the quadrotor can reach around the requested target point while avoiding the obstacles.**

***Index Terms*—Kinodynamics, motion planning, aerial robot**

I. Introduction

Recently, there are many researches on autonomous locomotion for a quadrotor, which is the vertical takeoff and landing (VTOL) aerial robot with four rotors. For autonomous locomotion of a quadrotor, it needs to move and avoid obstacles while keeping its attitude. There is a concept called "kinodynamic motion planning" which can consider kinematic constraints and dynamic constraints simultaneously [1], and some control methods based on kinodynamic motion planning are proposed [2]-[5].

Therefore, we aimed to realize "kinodynamic motion planning" of the quadrotor for designing the control input which considers kinematic constraints and dynamic constraints, simultaneously. In this research, the kinodynamic motion planning for the quadrotor is achieved by combining control input based on the harmonic potential field (HPF) for considering the obstacle information on the environment with nonholonomic control input for considering the dynamics of the quadrotor. By using the proposed method, it is already confirmed by simulations that the quadrotor can move to the arbitrary target point while avoiding obstacles and keeping its attitudes [6].

In this paper, we test the proposed kinodynamic motion planning, which was confirmed in only the simulations, by an actual experiment. The experiment assumes that the quadrotor moves in the static environment, and it is confirmed that the quadrotor can reach around the requested target point while avoiding the obstacles. Moreover, a controller based on the HPF and the viscous damping force to save the speed is compared to a controller based on using only HPF, by checking the behavior of the quadrotor.

II. Kinodynamic Motion Planning for a Quadrotor

In the proposed method, kinodynamic motion planning is achieved by combining nonholonomic control input and the gradient information which is calculated from the HPF. The system input $\boldsymbol{U}=[U_1 U_2 U_3 U_4]^T$, which is constructed by nonholonomic control input $\boldsymbol{u}_c$ and control input $\Delta\boldsymbol{u}$ based on the gradient of the HPF, is as follows:

$$\boldsymbol{U}=\boldsymbol{u}_c+\Delta\boldsymbol{u} \tag{1}$$

Here, U_1 is a control input for acting on each translational motion, and U_2 , U_3 and U_4 are control inputs for acting on roll angle ϕ, pitch angle θ and yaw angle ψ , respectively. In the following subsections, we describe the dynamical model of an quadrotor, the control input based on nonholonomic control $\boldsymbol{u}_c$ and the control input $\Delta\boldsymbol{u}$ based on the gradient of an HPF.

A. Dynamical Model of a Quadrotor

A quadrotor controls its three directional positions (x, y, z), in which it moves back-and-forth, right-and-left and up-and-down, and three attitude angles (ϕ, θ, ψ), in which it performs roll, pitch and yaw motion, by using mounted 4 rotors on the airframe. The coordinate (x, y, z) and the rotation angle (ϕ, θ, ψ) constitute the right-handed system. Let define m [kg] as the mass of the quadrotor, l [m] as the length from the center of the airframe to the center of the rotor, g [m/s2] as the gravity acceleration, I_x, I_y and I_z [kg/m2] as the moment of inertia around each axis respectively, and J_r [kg/m2] as the moment of inertia for a rotor. Here, U_1 is the control input for acting on each translational motion, and U_2, U_3 and U_4 are the control inputs for acting on roll, pitch and yaw motions, respectively. The dynamical model of the quadrotor is:

$$\begin{aligned}
\ddot{x} &= -(\cos\phi\sin\theta\cos\psi + \sin\phi\sin\psi)\frac{1}{m}U_1 \\
\ddot{y} &= -(\cos\phi\sin\theta\sin\psi - \sin\phi\cos\psi)\frac{1}{m}U_1 \\
\ddot{z} &= -g + (\cos\phi\cos\theta)\frac{1}{m}U_1 \\
\ddot{\phi} &= \dot{\theta}\dot{\psi}\left(\frac{I_y - I_z}{I_x}\right) - \frac{J_r}{I_x}\dot{\theta}\Omega + \frac{l}{I_x}U_2 \\
\ddot{\theta} &= \dot{\phi}\dot{\psi}\left(\frac{I_z - I_x}{I_y}\right) - \frac{J_r}{I_y}\dot{\phi}\Omega + \frac{l}{I_y}U_3 \\
\ddot{\psi} &= \dot{\phi}\dot{\theta}\left(\frac{I_x - I_y}{I_z}\right) + \frac{1}{I_z}U_4
\end{aligned} \tag{2}$$

B. Nonhlonomic Control Input

The control input $\boldsymbol{u}_c = [u_{c1}\, u_{c2}\, u_{c3}\, u_{c4}]^T$ is added for Z-direction and three attitude angle and given as follows[7]:

$$\begin{aligned}
u_{c1} &= \frac{mg}{\cos\phi\theta} - \frac{m\hat{U}_1}{\cos\phi\theta} \\
u_{c2} &= -\frac{I_x}{l}(\phi - \phi_T) - k_1\dot{\phi} \\
u_{c3} &= -\frac{I_y}{l}(\theta - \theta_T) - k_2\dot{\theta} \\
u_{c4} &= -I_z(\psi - \psi_T) - k_3\dot{\psi}
\end{aligned} \tag{3}$$

where $\hat{U}_1$ is

$$\hat{U}_1 = k_4(z - z_T) + k_5\dot{z} \tag{4}$$

In this equation, $k_1,..., k_5$ are positive constant gains, and z_T is an arbitrary altitude and (ϕ_T, θ_T, ψ_T) are the desired angles.

C. Added Control Input

In this subsection, an added control input $\Delta\boldsymbol{u}$ is described for the translational motion. In this paper, it is assumed that the quadrotor moves on X-Y plane while hovering in constant altitude. For the control in the X-Y plane, the X- and Y-directional gradients of an HPF are added in the control input for θ and ϕ angles. When the position coordinate of the quadrotor is $\boldsymbol{x} = [x\,y\,z]^T$ and the gradient of the HPF is $\nabla V(\boldsymbol{x}) = [f_x\; f_y\; f_z]^T$, then, using the gradient of the HPF, an added control input $\Delta\boldsymbol{u}$ is designed by

$$\Delta\boldsymbol{u} = -B_c\dot{\boldsymbol{x}} - K_v\nabla V(\boldsymbol{x}) \tag{5}$$

Here, $B_c \in \Re^{4\times3}$ and $K_v \in \Re^{4\times3}$ are the speed selection gain and the gradient selection gain of the HPF, respectively. The selection method of the selection gains depends on the movement characteristics and the form of the dynamic control law of the controlled object. The quadrotor can move its position by tilting the attitude. For example, in the X-Y plane, the quadrotor can move toward the X-axis by tilting the body to $-\theta$ angle, and move toward the Y-axis by tilting the body to ϕ angle. Therefore, it is assumed that the quadrotor is hovering in constant altitude using a nonholonomic controller. At that time, the control toward the X-Y direction can be achieved by adding the X- and Y-directional gradients of the HPF to the pitch (θ directional) controller u_{c3} and the roll (ϕ directional) controller u_{c2}, which are based on nonholonomic control.

According to the above discussions, if the quadrotor only moves on the X-Y plane, then the selection gains B_c and K_v can be decided as below:

$$B_c = \begin{bmatrix} 0 & 0 & 0 \\ 0 & b_c & 0 \\ b_c & 0 & 0 \\ 0 & 0 & 0 \end{bmatrix}, \quad K_v = \begin{bmatrix} 0 & 0 & 0 \\ 0 & k_v & 0 \\ k_v & 0 & 0 \\ 0 & 0 & 0 \end{bmatrix} \tag{6}$$

where, $k_v > 0$. Using the extended coordinate vector $\boldsymbol{x}_e \in \Re^{4\times3}$ and the extended gradient vector $\nabla V_e(\boldsymbol{x}) \in \Re^{4\times3}$, the control input based on the gradient of the HPF can be written by:

$$\Delta\boldsymbol{u} = -b_c\dot{\boldsymbol{x}}_e - k_v\nabla V_e(\boldsymbol{x}) \tag{7}$$

Here, $\dot{\boldsymbol{x}}_e = [0\,\dot{y}\,\dot{x}\,0]^T$ and $\nabla V_e(\boldsymbol{x}) = [0\, f_y \;\; f_x\, 0]^T$.

III. THE SPCIFICATION OF THE AR.DRONE

In this experiment, the AR. Drone 2.0 developed by Parrot Co. is used as the controlled object. Figure 1 shows the overview of the AR. Drone. The size of the frame is 32 (length) × 28 (width) [cm], and its weight is 400 [gf]. In addition, small cameras are mounted on the front and under the frame. The AR. Drone can keep the hovering state by controlling the attitude angle and its angular velocity with the mounted ATMEGA8L 8bit micro controller. This controller can receive the velocity toward each axis direction, V_X, V_Y, and, V_Z, a target altitude z^d, and ψ angle speed V_Ψ, as the control input from outside [8].

In this experiment, it is assumed that this attitude controller is equivalent to a nonholonomic controller in our method, and the additional controllers based on an HPF, NADFs, and clamping control function are added. In other

p-ISSN: 2356-5314
e-ISSN: 2460-075X

words, the kinodynamic motion planning is realized by giving the control inputs added on the ϕ and θ in our proposed method as the control inputs of V_Y and V_X for AR. Drone. Finally, the control inputs can be derived as follows:

Fig. 1. The picture of the AR. Drone

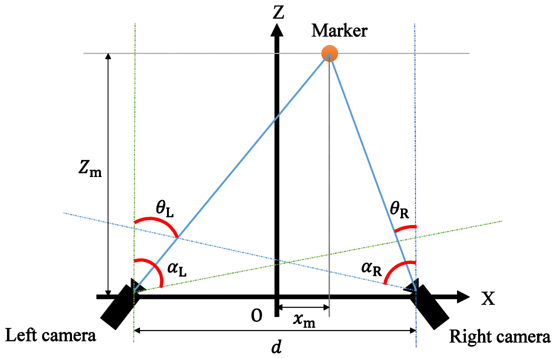

Fig. 2. Position measurement in X-Z plane.

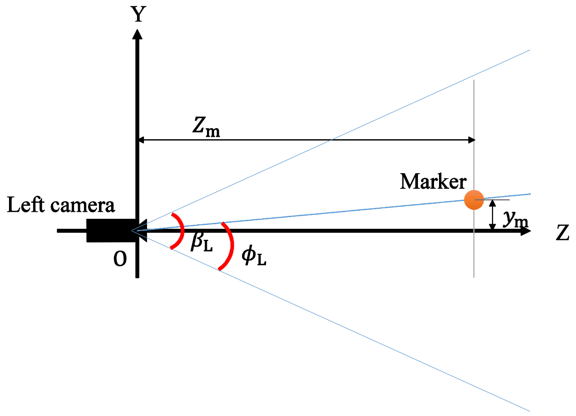

Fig. 3. Position measurement in Y–Z plane.

$$
\begin{aligned}
U_1 &= \frac{mg}{\cos\phi\theta} - \frac{m\hat{U}_1}{\cos\phi\theta} \\
U_2 &= -\frac{I_x}{l}(\phi - \phi_T) - k_1\dot{\phi} - b_c\dot{y} - k_v f_y \\
U_3 &= -\frac{I_y}{l}(\theta - \theta_T) - k_2\dot{\theta} - b_c\dot{x} - k_v f_x \\
U_4 &= -I_z(\psi - \psi_T) - k_3\dot{\psi}
\end{aligned} \tag{8}
$$

IV. Position Measurement System Using two Cameras

In the position measurement system used in this research, two cameras track the position of an infrared LED marker mounted on the AR. Drone, and the frame position is calculated [9]. Using the principle of triangulation based on the measured position, the 3D position of the marker (x, y, z) [cm] can be calculated on the coordinates, whose origin $O(0,0,0)$ is defined at the intermediate point between two cameras.

Figure 2 shows the overview of the position measurement system, which is based on using a stereo vision, for the horizontal and depth directional positions. It is assumed that the horizontal resolution of a camera image is defined by u_{max} , the horizontal angle of view for the camera of each right and left is defined as α_R and α_L , and the horizontal position of the marker on the camera image of each right and left is set to u_R and u_L , respectively. Then, θ_L , which is the angle from the left end of the horizontal angle of view for the left camera to the marker and θ_R , which is the angle from the right end of the horizontal angle of view for the right camera to the marker, can be expressed as follows:

$$\theta_L = \frac{u_L}{u_{max}} \alpha_L \tag{2}$$

$$\theta_R = \frac{u_{max} - u_R}{u_{max}} \alpha_R \tag{3}$$

Here, the horizontal position x_m and the depth directional position z_m can be shown by using the distance d between the right and left cameras:

$$x_m = z_m \tan\theta_L - \frac{d}{2} \tag{4}$$

$$z_m = d \frac{\cos\theta_L \cos\theta_R}{\sin(\theta_L + \theta_R)} \tag{5}$$

Figure 3 shows the overview of the vertically directional position measurement system using the stereo vision. When the two cameras are set horizontally, the horizontal position will become equal on each camera image, even in right and left cameras. When setting the left camera as the basis and assuming that the vertical angle of view of the left camera as β_L and the vertical position of the marker on the left camera image as v_L , the ϕ_L , which is the angle from the lower end of the vertical angle of view of the left camera to a marker, and y_m , which is the vertical position of the marker, can be represented as follows:

$$\phi_L = \frac{v_{max} - v_L}{v_{max}} \beta_L \tag{6}$$

$$y_m = z_m \tan\left(\phi_L - \frac{\beta_L}{2}\right) \tag{7}$$

p-ISSN: 2356-5314
e-ISSN: 2460-075X

Here, the average of the measured altitude from the right and left cameras is used as the marker position y_m, because there are some errors between the right and left cameras in the actual measurement. Assume that the vertical angle of view of the right and left cameras as β_R and β_L, the vertical position of the marker on the right camera image as v_R, the angle ϕ_R from the lower end of the vertical angle of view for the right camera to a marker, and the vertical position of the marker y_m, can be given as follows:

$$\phi_R = \frac{v_{\max} - v_R}{v_{\max}} \beta_R \tag{9}$$

$$y_m = \frac{z_m \tan\left(\phi_L - \frac{\beta_L}{2}\right) + z_m \tan\left(\phi_R - \frac{\beta_R}{2}\right)}{2} \tag{10}$$

In this research, this system is used for measuring the position of the AR. Drone from outside. Experiments

In this section, the actual moving experiments is conducted using the AR. Drone based on the proposed control input. As mentioned above, in this experiment, it is assumed that the mounted attitude controller on the AR. Drone is equal to the nonholonomic controller for keeping its attitude in our method, so that the added controllers based on an HPF, NADFs, and clamping control function are only added for guiding. Then, the target speed toward each axis, i.e., V_{XR}, V_{YR}, and V_{ZR}, are given as the control inputs for AR. Drone:

$$\begin{cases} -V_{X_R} = -b_{cx}\dot{y} - k_{vx} f_y \\ V_{Y_R} = -b_{cy}\dot{x} - k_{vy} f_x \end{cases} \tag{11}$$

Note that, b_{cx}, b_{cy}, k_{vx}, and k_{vy} are the positive constant gains, and f_x and f_y are the gradients toward X- and Y-direction calculated from an HPF. Here, as mentioned later, V_{XR} is set to a negative value for adjusting the difference between the robot axis system and the coordinate system of the position measurement system.

In this experiment, the marker for measuring a position is mounted on a frame as in Fig. 4, and the position of the marker is measured by two cameras set in the environment for confirming that the proposed controller can guide the quadrotor to the target point. The gradient of an HPF is calculated by desktop PC, and the data is sent to the AR. Drone through the Wi-Fi. The HPF is the potential field which is calculated from the reaction force from the obstacles and the attractive force from the target point. In this experiment, the environment is assumed to be known, and the HPF that was created in advance is used. For checking the detail of the HPF, see the paper [6].

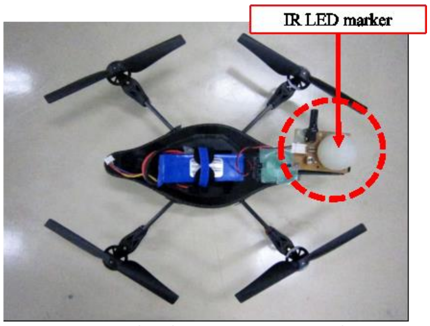

Fig. 4. Example of a figure caption. *(figure caption)*

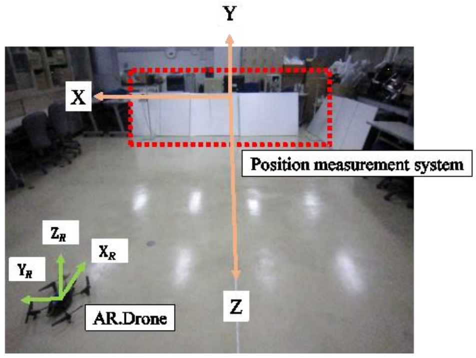

Fig. 5. Example of a figure caption. *(figure caption)*

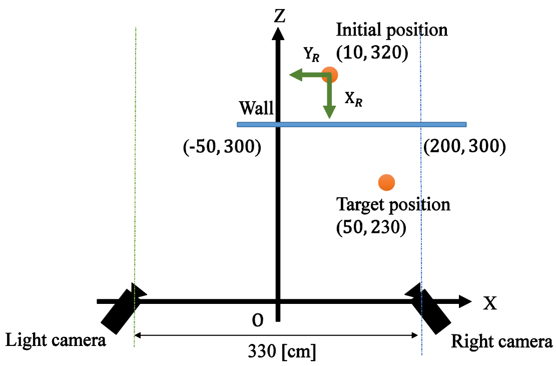

Fig. 6. Example of a figure caption. *(figure caption)*

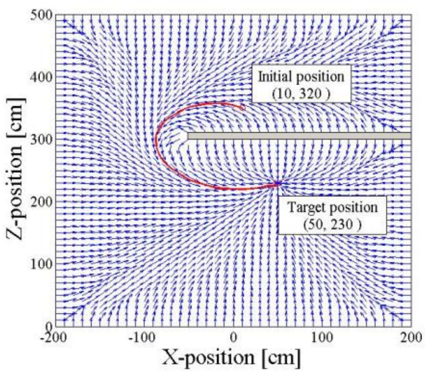

Fig. 7. Example of a figure caption. *(figure caption)*

p-ISSN: 2356-5314
e-ISSN: 2460-075X

A. Conditions

Figure 5 shows the picture of an actual environment, and Fig. 6 shows the position relation in an experimental environment as viewed from the top. As shown in Fig. 6, the initial position of the AR. Drone is set that the positive directions of the X-, Y-, and Z-axis of the position measurement system are matched with the positive directions of the Y_R- and Z_R-axis, and the negative direction of the X_R-axis of the robot coordinate system, respectively. Moreover, as shown in Fig. 6, the distance between the cameras is set to 3.3 [m]. Then, the AR. Drone took off at the initial position $(x_0, z_0) = (10, 320)$ [cm] and moved toward the target position $(x_T, z_T) = (50, 230)$ [cm], and the trajectory of it was recorded. The target angular velocity in yaw motion was always set to 0 [rad/s], the target altitude was set to 0 [cm], and the takeoff and landing motion was performed manually. The grid size of HPF was set to 5×5 [cm]. The normalized gradient vector field and the ideal trajectory of the experimental environment are shown in Fig. 7.

In this experiment, the results by using the HPF and the viscous damping force are compared with the results obtained by using only the HPF to confirm the effect of the viscous damping force. Therefore, the gains are set to $b_{cx} = 0.001$ and $b_{cy} = 0.0005$ when using the viscous damping force, and set to $b_{cx} = b_{cy} = 0.0$ when not using the viscous damping force. The gains for the gradient of the HPF are always set as $k_{vx} = 0.01$ and $k_{vy} = 0.02$, respectively. The gain for V_x is set to be larger than the gain for V_y, because the inertial moments of AR. Drone around the X- and Y-axes are different, and there is a difference in the control effect [10].

B. Results

The results of the flight experiment are shown in Figs. 8 - 12. Figure 8 shows the trajectory of the quadrotor on X-Z plane. Moreover, Figs. 9 - 11 show the change of the positions of X, Y and Z directions, whereas Fig. 12 shows the error from the target position. In each graph, the blue solid lines show the results with viscous damping force, whereas the orange broken lines show the results without viscous damping force. The red solid lines in each graph show the target value.

C. Discussions

As shown in Figs. 8-12, it is confirmed that the quadrotor was able to reach the target position with both controllers while avoiding the obstacle. Moreover, as shown in Fig. 11, the both controllers were able to keep the altitude of the quadrotor within ± 10 [cm] from the target altitude.

The controller with the viscous damping force was able to guide the quadrotor to the target point a little faster than the case using the controller without viscous damping force. This is attributed to the fact that the viscous damping force saved the overshoot and the controller was able to guide the quadrotor to the target point with less movement. There is a possibility that the viscous damping force works more effective by tuning the gains.

V. CONCLUSIONS

In this paper, actual experiments have been made to implement the kinodynamic motion planning based on an HPF to an actual machine. In particular, assuming that the attitude controller mounted on the AR. Drone developed by Parrot Co. is equivalent to the nonholonomic controller in our method, the controller based on the gradient of an HPF was added for guiding the AR. Drone. Then, the trajectory of the quadrotor was measured and recorded by using a cameras system mounted on the environmental side. From the actual experimental results, it was confirmed that the AR. Drone was able to move to an arbitrary target point while keeping its attitude angles and avoiding the obstacle. Moreover, it was shown that there exists a possibility to realize more effective control by adding the viscous damping force.

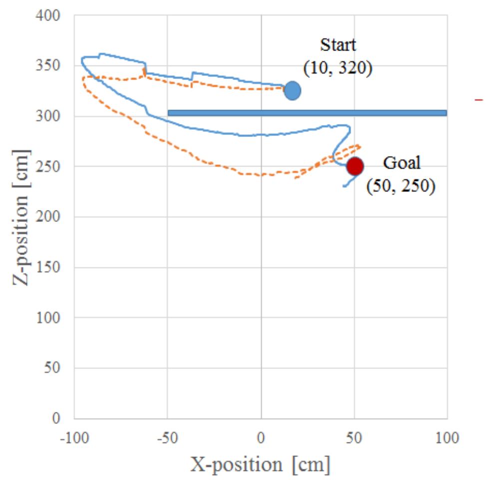

Fig. 8. Trajectory of the quadrotor on X-Z plane

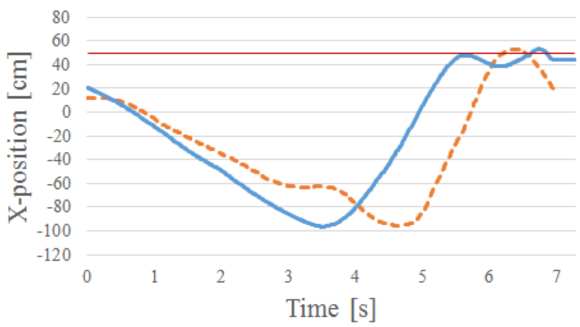

Fig. 9. Time response of X position of the quadrotor

p-ISSN: 2356-5314
e-ISSN: 2460-075X

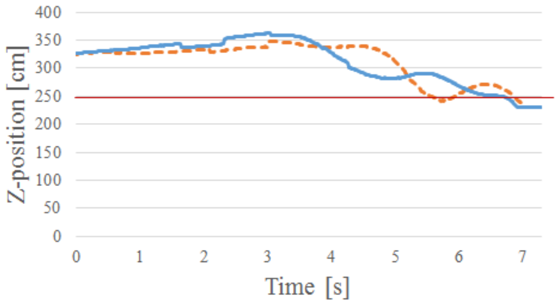

Fig. 10. Time response of Z position of the quadrotor

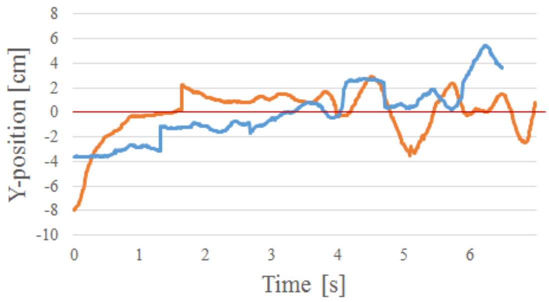

Fig. 11. Time response of Y position (altitude) of the quadrotor

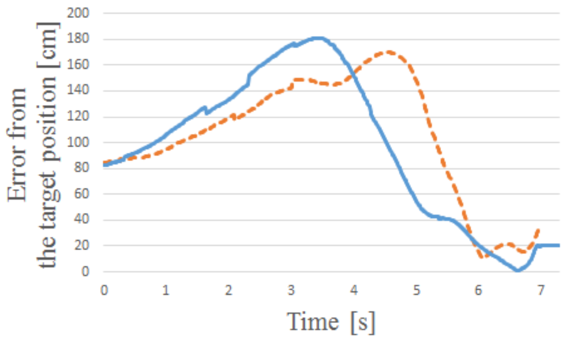

Fig. 12. Error from the target position

[1] B. Donald, P. Xavier, J. Canny, and J. Reif, "Kinodynamic motion planning," J. of the ACM, vol. 40, no. 5, pp. 1048-1066, 1993.

[2] S. M. LaValle and J. J. Kuffner: "Randomized kinodynamic planning", Int. J. of Robotics Research, vol. 20, no. 5, pp. 378-400, 2001.

[3] Q. Pham, S. Caron, and Y. Nakamura, "Kinodynamic planning in the configuration space via admissible velocity propagation," Proc. of Robotics: Science and Systems, 2013.

[4] E. Rimon and D. Koditschek, "Exact robot navigation using artificial potential functions," IEEE Trans. on Robotics and Automation, vol. 8, no. 5, pp. 501-518, 1992.

[5] J. Peng and S. Akella, "Coordinating multiple robots with kinodynamic constraints along specified paths," Int. J. of Robotics Research, Vol. 24, No. 4, pp. 295--310, 2005.

[6] K. Motonaka, K. Watanabe and S. Maeyama, "Kinodynamic motion planning and control using anisotropic damping forces," in Proc. of Int. Symp. on Artificial Life and Robotics (AROB), 2013.

[7] S. Bouabdallah, P. Murrieri, and R. Siegwart, "Design and control of an indoor micro quadrotor," IEEE Robotics and Automation Magazine, vol. 5, pp. 4393-4398, 2004.

[8] P. Bristeau, F. Callou, D. Vissiere, and N. Petit, "The navigation and control technology inside the AR.Drone micro UAV," Preprint of 18th IFAC World Congress, pp. 1477-1484, 2011.

[9] K. Watanabe, Y. Yamada, and I. Nagai, "The development of a 3D position measurement system for indoor aerial robots," Proc. of 2014 14th Int. Conf. on Control, Automation and Systems (ICCAS 2014), pp.1185-1190, 2014.

[10] J. Pestana Puerta, J. L. Sanchez-Lopez, I. Mellado Bataller, C. Fu, and P. Campoy Cervera, "AR drone identification and navigation control at CVG-UPM," Proc. of CEA XXXIII Jornadas de Automatica 2012.